BROADBAND LOCALIZATION IN A DISPERSIVE MEDIUM THROUGH SPARSE WAVENUMBER ANALYSIS

Joel B. Harley, José M.F. Moura

Carnegie Mellon University
Department of Electrical and Computer Engineering
Pittsburgh, PA 15213

ABSTRACT

Matched field processing is a powerful tool for accurately localizing targets in dispersive media. However, matched field processing requires a precise model of the medium under test. In underwater acoustics, where matched field processing has been extensively studied, authors often resort to extremely detailed numerical models of the propagation medium, which are computationally expensive and impractical for many applications. As an alternative, this paper uses convex sparse recovery techniques to construct, directly from measured data, an accurate model of a plate medium based on its dispersion characteristics. From this data-driven model, the Green's function between two points can be readily predicted. We demonstrate the effectiveness of this model by localizing a source in a dispersive plate medium. The results visually illustrate our approach to significantly improve localization accuracy and reduce artifacts when compared to a conventional narrowband technique.

Index Terms— Sparse recovery, matched field processing, time reversal, localization, inverse problems

1. INTRODUCTION

Many applications in acoustics are concerned with locating targets in complex media with multi-modal and dispersive characteristics. In these media, a single propagating wave is represented by a superposition of wave modes, each traveling at a different velocity that varies as a function of frequency. These types of waves include Love waves and Rayleigh waves [1] in seismology, Lamb waves and pipe waves [2] in non-destructive evaluation and structural health monitoring, and Pekeris shallow water waves [3] in underwater acoustics.

For complex media, matched field processing [4, 5, 6] and time reversal [7, 8] have been widely studied for high resolution localization. However, matched field processing requires a detailed model of the environment and its Green's function. In underwater acoustics, where it has been extensively studied, matched field processing usually requires a detailed numerical model based on the wave equation [5]. However, these models are usually expensive and impractical for most applications. In time reversal, the Green's function is instead measured directly from the medium [7]. This too, however, is impractical for many applications.

In this paper, we construct an accurate model of the Green's function for an aluminum plate directly from measured data through the use of sparse recovery techniques developed for compressed sensing applications [9, 10, 11]. We accomplish this by transforming the data into a sparse frequency-wavenumber representation that is invariant to sensor positions on the surface of the plate. We refer to this as *sparse wavenumber analysis* (SWA). This position-invariant representation is then used to predict the Green's function between any points in the medium. We refer to this as *sparse wavenumber synthesis* (SWS). We expand on our previous work [12] by integrating this data-driven model with matched field processing to localize a source in the dispersive plate medium.

2. PROBLEM FORMULATION

In this section, we briefly discuss the general model used to characterize Lamb waves, waves that propagate through a plate. From this model, we show that Lamb waves are characterized by their frequency-wavenumber representation, which is invariant to sensor position. We then represent the frequency-wavenumber representation as the solution to an underdetermined linear inverse problem.

2.1. Lamb wave model

We consider a general model for the voltage, generated by Lamb waves, measured by a collection of point-size piezoelectric transducers on a single surface of a plate with a finite height and unbounded length and width. We can approximately represent the voltage by the Green's function $X(r, \omega)$, which is dependent on angular frequency ω and the distance

This material is based upon work supported by the National Defense Science and Engineering Graduate Fellowship and the National Science Foundation Graduate Research Fellowship under Grant No. 0946825.

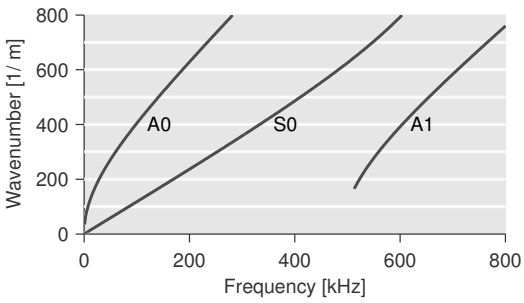

Fig. 1. Portion of the theoretical dispersion curves for the zeroth order antisymmetric (A0), the zeroth order symmetric (S0), and the first order antisymmetric (A1) modes of an unbounded aluminum plate.

between any two transducers r, such that [12, 13, 14]

$$X(r,\omega) = \sum_m \frac{1}{\sqrt{k_m(\omega) r}} S(\omega) G_m(\omega)\, e^{-j k_m(\omega) r} \ . \quad (1)$$

In (1), $X(r,\omega)$ is a summation of wave modes, each with a complex-valued, frequency-dependent amplitude $G_m(\omega)$ and frequency-dependent wavenumber $k_m(\omega)$. The term $S(\omega)$ is the known frequency response of the transmitted signal.

The function $k_m(\omega)$ is also known as the dispersion relation for the wave mode [2]. The collection of all dispersion relations is known as the dispersion curves for the medium. Fig. 1 illustrates an example portion of the theoretical dispersion curves for an aluminum plate, determined by numerically solving the Rayleigh-Lamb equations [2].

Notice that from $G_m(\omega)$ and $k_m(\omega)$, which are invariant of the sensor positions, we can synthesize the Green's function for any distance. While the theoretical values of $G_m(\omega)$ and $k_m(\omega)$ can be numerically obtained for Lamb waves, the results are dependent on prior knowledge of the mediums material parameters. These parameters are often unknown and their values may vary with the condition of the sensors [15] and changes in the environment, such as temperature [16].

2.2. Discrete, linear formulation

We now discretize the continuous model in (1) and represent it as a discrete, linear system. To accomplish this, we assume we observe N discrete wave measurements corresponding to travel distances $\mathbf{r} = [r_1, \ldots, r_N]^T$. This is equivalent to discretizing $X(r,\omega)$ across N distances. We then uniformly discretize $X(r,\omega)$ across Q angular frequencies $\omega_1, \ldots, \omega_Q$ to represent the measurements as an $N \times Q$ matrix

$$\mathbf{X}(\mathbf{r}) \quad = \quad [X(r_i, \omega_j)]_{ij} \ . \quad (2)$$

We also recognize that the dispersion relations $k_m(\omega)$ and their associated amplitudes $G_m(\omega)$, for every m, can be represented as a single, two-dimensional function in frequency-wavenumber (ω-κ) space

$$V(\kappa,\omega) = \begin{cases} S(\omega) G_m(\omega) & \text{if } \kappa = k_m(\omega) \text{ for any } m \\ 0 & \text{otherwise} \end{cases} \ . \quad (3)$$

We now uniformly discretize $V(\kappa,\omega)$ across Q angular frequencies $\omega_1, \ldots, \omega_Q$ and across K wavenumbers $\kappa_1, \ldots, \kappa_K$ to form a $K \times Q$ matrix

$$\mathbf{V} \quad = \quad [V(\kappa_i, \omega_j)]_{ij} \ . \quad (4)$$

It can now be shown that the measurements $\mathbf{X}(\mathbf{r})$ and their frequency-wavenumber representation $\mathbf{V}$ can be represented by the discrete, linear relationship

$$\mathbf{X}(\mathbf{r}) \quad = \quad \mathbf{D}_r(\mathbf{r}) \mathbf{A}(\mathbf{r}) \mathbf{D}_k \mathbf{V} \quad (5)$$

$$\mathbf{A}(\mathbf{r}) \quad = \quad \left[e^{-j \kappa_j r_i} \right]_{ij} \quad (6)$$

$$\mathbf{D}_r(\mathbf{r}) \quad = \quad \text{diag} \left[r_1^{-1/2}, \ldots, r_N^{-1/2} \right] \quad (7)$$

$$\mathbf{D}_k \quad = \quad \text{diag} \left[\kappa_1^{-1/2}, \ldots, \kappa_K^{-1/2} \right] \ . \quad (8)$$

In (5), the matrix $\mathbf{A}(\mathbf{r})$ is an $N \times K$ generalized Vandermonde matrix, representing the complex exponential term in (1) at discretized distances and wavenumbers. The matrices $\mathbf{D}_r$ and $\mathbf{D}_k$ are $N \times N$ and $K \times K$ diagonal matrices, respectively, that represent the geometric spreading factors in (1). Intuitively, the matrix $\mathbf{A}(\mathbf{r})$ maps each column, or frequency, of $\mathbf{V}$ from a distance domain onto a wavenumber domain.

3. SPARSE WAVENUMBER PROCESSING

Our goal now is to accurately estimate the frequency-wavenumber representation $\mathbf{V}$ that is invariant of all possible distances $\mathbf{r}$. However, to obtain a sufficiently fine resolution in the frequency-wavenumber domain, we usually require that $K > N$. This implies that (5) represents an underdetermined system and there exists an infinite number of solutions $\mathbf{V}$.

3.1. Sparse wavenumber analysis

Although many possible solutions $\mathbf{V}$ exist, we know that the true position-invariant solution exhibits a special property over continuous space. That is, the continuous frequency-wavenumber representation $V(\kappa,\omega)$ in (3) is sparse, or mostly zeros. Therefore, we can assume the sparsest solution for $\mathbf{V}$ is approximately the true solution.

Based on recent efforts in the study of compressed sensing [10, 11], we know that we can obtain a sparse approximate solution to (5) through an optimization known as basis pursuit denoising [9, 17]. We use basis pursuit denoising rather than the standard basis pursuit [9] because we assume our measurements will be corrupted by noise. Therefore, we define our basis pursuit denoising solution with a given $\mathbf{r}$ as

$$\mathbf{D}_k \mathbf{V} = \arg\min_{\mathbf{V}} \|\mathbf{A}\mathbf{V} - \mathbf{D}_r^{-1} \mathbf{X} \mathbf{D}_E\|_F^2 + \lambda \|\mathbf{V}\|_1 \ . \quad (9)$$

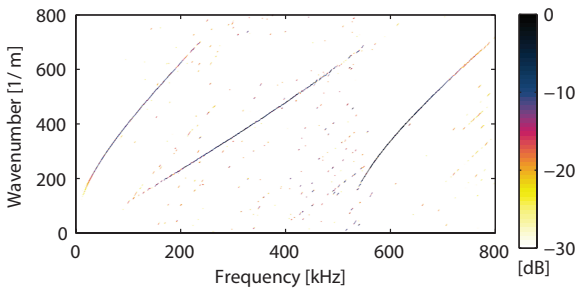

Fig. 2. The frequency-wavenumber representation, computed using basis pursuit denoising, of experimentally measured Lamb waves.

In (9), the λ parameter is a chosen scalar that balances the emphasis between the squared error term, which encourages model fitness, and the ℓ_1 norm, which emphasizes sparsity. The matrix $\mathbf{D}_E$ is a diagonal $Q \times Q$ matrix that normalizes the columns of $\mathbf{D}_r^{-1}\mathbf{X}$ to have unit norm. This matrix is included to improve the consistency of our choice of λ.

Note that (9) is equivalent to computing the basis pursuit denoising solution for each column of $\mathbf{V}$ individually. This is how $\mathbf{V}$ is computed in practice. However, we retain the matrix notation here for conciseness.

Figure 2 shows an example frequency-wavenumber representation $\mathbf{V}$ computed from experimental Lamb wave measurements. We visually observe that this result closely resembles the dispersion curves shown in Figure 1.

3.2. Sparse wavenumber synthesis

We can now use our frequency-wavenumber representation $\mathbf{V}$ of the measurements to predict the Green's function between other points in the medium. This process is expressed by

$$\widehat{\mathbf{X}}(\widehat{\mathbf{r}}) \quad = \quad \mathbf{D}_r(\widehat{\mathbf{r}})\mathbf{A}(\widehat{\mathbf{r}})\mathbf{D}_k\mathbf{V}\ , \tag{10}$$

where $\widehat{\mathbf{X}}(\widehat{\mathbf{r}})$ represents the predicted Green's functions for a chosen collection of $\widehat{N}$ distances $\widehat{\mathbf{r}} = [\widehat{r}_1, \ldots, \widehat{r}_{\widehat{N}}]^T$.

4. MATCHED FIELD PROCESSING

We now consider a new collection of M measurements

$$\mathbf{Y} \quad = \quad [X(\rho_i, \omega_j)]_{ij} \tag{11}$$

that represent waves originating from a single point source and traveling unknown distances $\rho = [\rho_1, \ldots, \rho_M]^T$ to M sensors. Our objective is to locate this point source. To accomplish this task, we combine the predictive power of SWA and SWS with matched field processing.

4.1. Sparse wavenumber processing

We integrate our predictions $\widehat{\mathbf{X}}(\widehat{\mathbf{r}})$ with matched field processing by using the predictions as the Green's function model for the matched field processor. Therefore, the coherent matched field location estimate [6], which is a minimum squared error estimate, is defined by

$$\widehat{\rho} = \arg\max_{\widehat{\mathbf{r}}} b(\widehat{\mathbf{r}}) \tag{12}$$

where $b(\widehat{\mathbf{r}})$ is the coherent ambiguity function [6]

$$b(\widehat{\mathbf{r}}) \quad = \quad \frac{\left|\mathrm{tr}\left(\mathbf{Y}^H\widehat{\mathbf{X}}(\widehat{\mathbf{r}})\right)\right|^2}{\|\widehat{\mathbf{X}}(\widehat{\mathbf{r}})\|_F^2}\ . \tag{13}$$

This processing strategy is also known as time reversal [7] or backpropagation because, intuitively, it propagates a time-reversed replica of the received signals $\mathbf{Y}$ backward into the medium, which is simulated by $\widehat{\mathbf{X}}(\widehat{\mathbf{r}})$.

4.2. Narrowband delay processing

For comparison, we also consider a conventional narrowband Green's function model. For multi-modal and dispersive media, localization is usually processed using a narrow band of frequencies with a single dominating mode and an approximately constant group velocity [18, 19]. These methods usually use a simple Green's function model based on delays

$$\widehat{\mathbf{X}}(\widehat{\mathbf{r}}) \quad = \quad \left[S(\omega_j)e^{-j\omega_j\widehat{r}_i/v_g}\right]_{ij}\ , \tag{14}$$

where $S(\omega)$ is the known transmission signal and v_g is the dominating wave mode's group velocity. This Green's function model is also integrated with the coherent matched field processor in (12) and (13) to localize the source.

5. EXPERIMENTAL SETUP

We consider an aluminum plate specimen with a 1.22 m by 1.22 m by 0.2844 cm length, width, and thickness. Bonded to the plate's surface are 17 synchronized 0.7 cm by 0.8 cm piezoelectric transducers capable of transmitting and receiving ultrasonic waves. Figure 3 illustrates the positions of each sensor. To compute $\mathbf{V}$, we collect ultrasonic measurements corresponding to every combination of transmitter and receiver pairs from 16 of the 17 sensors. This results in a total of $N = 272$ measurements. We then collect $M = 16$ additional measurements from the 17th sensor for localization. Each sensor transmits a 10 μs long linear chirp signal with a bandwidth from 0 Hz to 2 MHz.

Since our model in (1) considers an unbounded plate while the experimental data is taken from a bounded plate, the data will be corrupted by significant interference from reflective boundaries. To reduce this interface when computing $\mathbf{V}$, we use a smooth time window to remove data

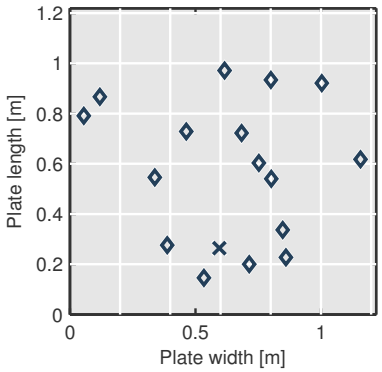

Fig. 3. Sensor locations for the experimental plate setup. Diamonds indicate the sensors used to estimate the medium's Green's function and to listen for sources. The cross indicates the source to locate.

corresponding to a direct path group velocity of 2000 m/s or less. Although significant interference remains, basis pursuit denoising is generally robust to it [12]. To localize the 17th sensor, we do not apply any time window to the data.

For implementing SWA, basis pursuit denoising is applied with a parameter of $\lambda = 0.4$ and is implemented using the convex optimization package CVX [20, 21].

6. RESULTS AND DISCUSSION

Figure 4(a) illustrates the ambiguity function $b(\widehat{\mathbf{r}})$ for the Green's function model in (13), predicted by SWA and SWS in (9) and (10). The frequency-wavenumber representation $\mathbf{V}$ obtained to synthesize the Green's function model is shown in Figure 2 with $K = 800$ wavenumbers and $Q = 800$ frequencies. The ambiguity function is computed from 40 frequencies uniformly spread from 20 kHz to 800 kHz.

Figure 4(b) illustrates the ambiguity function $b(\widehat{\mathbf{r}})$ for the delay based Green's function model in (14). The matched field processor uses 40 frequencies uniformly spread from 260 kHz to 340 kHz. The model uses a group velocity of 5110 m/s, which was obtained from the slope of the second dispersion curve in Figure 2.

Both plots show a 10 cm region of the plate. The light gray circle in the center in each plot represents the center of the 0.7 cm by 0.8 cm sensor of interest. The dark gray cross in each plot denotes the maximum value across the shown area, i.e. the estimated location of the source. Each plot is normalized so that the maximum value is 0 dB.

By visual inspection, the SWA predictions achieve much better localization. Our predictive model estimates the source to be only 0.14 cm away from the center of the transducer while the delay model exhibits an error of 3.37 cm. Figure 4(b) also shows that the delay model generates large artifacts

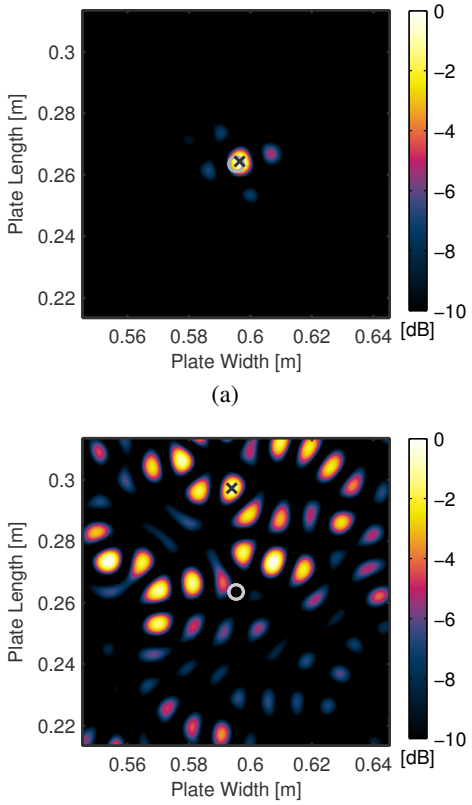

Fig. 4. Ambiguity functions generated from (a) a predictive sparse wavenumber analysis model and (b) a delay model. Circles indicate the true source location. Crosses indicate the matched field location estimates.

that may be mistaken for sources. In contrast, our predictive model in Figure 4(a) displays only a few weak artifacts.

7. CONCLUSIONS

This paper demonstrates how sparse wavenumber analysis and sparse wavenumber synthesis can predict the Green's function of a Lamb wave medium from a finite number of measurements. These techniques achieve this by transforming the data into a sparse frequency-wavenumber domain that is invariant of sensor position.

We integrate this predictive Green's function model with a coherent matched field processor to localize an acoustic source on an aluminum plate. When compared with a conventional narrowband delay model of the Green's function, the predictive sparse wavenumber analysis model provides more accurate localization and visually fewer artifacts. In future work, we plan to investigate how these results vary with the number of sensors and the degree of noise in the system.

8. REFERENCES

[1] J.D. Achenbach, *Wave Propogation in Elastic Solids*, Elsevier Science Publishers B.V., Amsterdam, 1975.

[2] K.F. Graff, *Wave Motion in Elastic Solids*, Dover Publications, New York, 1st ed. edition, 1991.

[3] F.B. Jensen, W.A. Kuperman, M.B. Porter, and H. Schmidt, *Computational Ocean Acoustics*, Springer New York, New York, NY, 2011.

[4] A.B. Baggeroer, "Matched field processing: Source localization in correlated noise as an optimum parameter estimation problem," *J. Acoust. Soc. Am.*, vol. 83, no. 2, pp. 571, 1988.

[5] A.B. Baggeroer, W.A. Kuperman, and P.N. Mikhalevsky, "An overview of matched field methods in ocean acoustics," *IEEE Journal of Oceanic Engineering*, vol. 18, no. 4, pp. 401–424, Oct. 1993.

[6] W. Mantzel, J. Romberg, and K. Sabra, "Compressive matched-field processing.," *J. Acoust. Soc. Am.*, vol. 132, no. 1, pp. 90–102, July 2012.

[7] W.A. Kuperman, W.S. Hodgkiss, H.C. Song, T. Akal, C. Ferla, and D.R. Jackson, "Phase conjugation in the ocean: Experimental demonstration of an acoustic time-reversal mirror," *J. Acoust. Soc. Am.*, vol. 103, no. 1, pp. 25–40, Jan. 1998.

[8] J.M.F Moura and Y. Jin, "Time reversal imaging by adaptive interference canceling," *IEEE Trans. Signal Process.*, vol. 56, no. 1, pp. 233–247, Jan. 2008.

[9] S.X. Chen, D.L. Donoho, and M.A. Saunders, "Atomic decomposition by basis pursuit," *SIAM J. Sci. Comput.*, vol. 20, no. 1, pp. 33, 1998.

[10] D.L. Donoho, "Compressed sensing," *IEEE Trans. Inf. Theory*, vol. 52, no. 4, pp. 1289–1306, Apr. 2006.

[11] E.J. Candès, J.K. Romberg, and T. Tao, "Stable signal recovery from incomplete and inaccurate measurements," *Comm. Pure Appl. Math.*, vol. 59, no. 8, pp. 1207–1223, Aug. 2006.

[12] J.B. Harley and J.M.F. Moura, "Sparse recovery of the multimodal and dispersive characteristics of Lamb waves," *J. Acoust. Soc. Am.*, under review.

[13] W. Gao, C. Glorieux, and J. Thoen, "Laser ultrasonic study of Lamb waves: Determination of the thickness and velocities of a thin plate," *Int. J. Eng. Sci.*, vol. 41, no. 2, pp. 219–228, Jan. 2003.

[14] J.S. Hall and J.E. Michaels, "A model-based approach to dispersion and parameter estimation for ultrasonic guided waves," *J. Acoust. Soc. Am.*, vol. 127, no. 2, pp. 920–930, Feb. 2010.

[15] X.P. Qing, H.-L. Chan, S.J. Beard, T.K. Ooi, and S.A. Marotta, "Effect of adhesive on the performance of piezoelectric elements used to monitor structural health," *Int. J. Adhes. Adhes.*, vol. 26, no. 8, pp. 622–628, Dec. 2006.

[16] J.B. Harley and J.M.F. Moura, "Scale transform signal processing for optimal ultrasonic temperature compensation," *IEEE Trans. Ultrason., Ferroelectr., Freq. Control*, vol. 59, no. 10, Oct. 2012.

[17] D.L. Donoho, M. Elad, and V.N. Temlyakov, "Stable recovery of sparse overcomplete representations in the presence of noise," *IEEE Trans. Inf. Theory*, vol. 52, no. 1, pp. 6–18, Jan. 2006.

[18] J.E. Michaels, "Detection, localization and characterization of damage in plates with an in situ array of spatially distributed ultrasonic sensors," *Smart Mater. Struct.*, vol. 17, no. 3, pp. 035035, June 2008.

[19] T. Clarke and P. Cawley, "Enhancing the defect localization capability of a guided wave SHM system applied to a complex structure," *Struct. Health Monit.*, vol. 10, no. 3, pp. 247–259, June 2010.

[20] M. Grant and S. Boyd, "Graph implementations for nonsmooth convex programs," in *Recent Advances in Learning and Control*, V. Blondel, S. Boyd, and H. Kimura, Eds., Lecture Notes in Control and Information Sciences, pp. 95–110. Springer-Verlag Limited, 2008.

[21] M. Grant and S. Boyd, "CVX: Matlab software for disciplined convex programming, version 1.21," Apr. 2011.